Evidence for various higher-subband resonances and interferences in a GaAs/AlAs asymmetric quadruple-quantum-well superlattice analyzed from its photoluminescence properties

Keisuke Hata,[1] Makoto Hosoda,[2] Kouichi Akahane,[3] and Naoki Ohtani[1]

[1]*Department of Electronics, Doshisha University, 1-3 Tatara-Miyakodani, Kyotanabe-shi, Kyoto 610-0321, Japan*

[2]*Research Institute of Electronics, Shizuoka University, Johoku 3-5-1, Naka-ku, Hamamatsu, Shizuoka 432-8011, Japan*

[3]*Photonic Network Research Institute, National Institute of Information and Communications Technology (NICT), 4-2-1 Nukui-Kitamachi, Koganei, Tokyo 184-8795, Japan*

(Received 29 February 2016; revised manuscript received 3 February 2017; published 22 February 2017; corrected 24 February 2017)

In this paper, we present evidence for the resonances between higher subbands in an asymmetric quadruple-quantum-well (AQQW) superlattice (SL) by photoluminescence (PL) spectra. Since each QW in an AQQW is separated by thin barriers, subband interferences can easily arise. As a result, various PL branches caused by the subband resonances are observed, including PL emissions from the higher-energy Γ states, the *X* state in a barrier with longitudinal optical phonon replica, and long-range Γ-*X* transfer with Γ-*X* mixing. However, in conventional QW systems, the PL emissions from higher-energy subbands and their interference have not been clearly observed yet; in our system, the interferences between higher-energy subbands can be observed through PL emission, since we achieved effective electron injection into the higher subbands under very thin barriers. From these observations, we exposed the existence of such interferences and transport processes.

DOI: 10.1103/PhysRevB.95.075309

I. INTRODUCTION

PL emission from the *X* state has been explained in terms of pseudodirect transition by Γ-*X* mixing in type-II quantum wells (QWs) [1–3]. After these studies, the carrier transport and the optical properties in biased direct-transition (type-I) GaAs/AlAs multiple quantum well (MQW) affected by Γ-*X* scattering were investigated [4–7]. However, the transport properties in the strongly coupled subbands and the remote Γ-*X* scattering (long-range interaction between the Γ states and the *X* state separated by several barriers) in these QW systems have not yet been clarified.

The asymmetric multiple-quantum-well (AMQW) structure can be designed to observe photoluminescence (PL) recombination processes from the higher-energy subbands associated with the Γ-*X* mixing. In these AMQW's, the interference between the subbands affects the PL emission spectra [4]. However, the resonances between higher subbands and their observations remain unclarified. In this report, we show evidence of resonances among higher subbands, long-range Γ-*X* transfers, and Γ-*X* mixing in an asymmetric quadruple-quantum-well (AQQW) superlattice (SL) by analysis of its PL spectra.

The designed sample is a GaAs/AlAs AQQW SL, which has *X* subband states in the AlAs barrier. We achieve carrier injection from the *X* state to higher-energy subbands by precisely controlling the higher-energy Γ and *X* subband energies.

In this paper, we analyze the bias-dependent PL spectra from an AQQW SL that was affected by the interference among higher-energy subbands and interactions with the *X* state. Since the AQQW studied here contains four QWs separated by thin AlAs barriers in one SL period, efficient carrier injection into the higher-energy states is expected by applying a bias voltage due to strong coupling between the electron wave functions among these four QWs. We show the Γ-*X* transfer and mixing between higher-energy electron subbands with their interferences and the *X* state in a strongly coupled AQQW SL.

II. SAMPLE STRUCTURE

The sample used here was grown on a (100) n^+-GaAs substrate by molecular beam epitaxy (MBE). An undoped 20-period AQQW SL was embedded in the *i* layer of a *p*-*i*-*n* diode structure. The growth sequence was a 300-nm n^+-GaAs buffer layer, a 700-nm n-$Al_{0.4}Ga_{0.6}As$ cladding layer, a 50-nm undoped $Al_{0.4}Ga_{0.6}As$ cladding layer, an undoped 20-period AQQW SL, an undoped 11-ML (monolayer) AlAs layer, an undoped 50-nm $Al_{0.4}Ga_{0.6}As$ cladding layer, a 200-nm p-$Al_{0.4}Ga_{0.6}As$ cladding layer, and a 10-nm p^+-GaAs cap. The structure of one period of the AQQW SL was constructed of 10/12/2/12/2/8/2/8 ML thickness layers, which are named and numbered B1/Q1/B2/Q2/B3/Q3/B4/Q4 (Fig. 1), where B and Q, respectively, correspond to the AlAs barrier and the GaAs QW. However, the real sample grown had 11/12/2/12/2/8/2/8 ML-thick layers (Fig. 1) by a monolayer fluctuation, which is common for MBE growth. In this condition, the experimental PL wavelength and the PL branches were consistent with the subband resonance voltages calculated from the transfer-matrix method.

Note that the four QWs in one period were separated by the thin 2-ML AlAs barriers, resulting in strong coupling between wave functions. A wide 11-ML barrier (B1) separated each SL period. The subbands are defined as follows. Hereafter, as shown in Fig. 2(a), the Γ subbands in the AQQW SL are indexed as Γ*mn*, where "*m*" denotes the QW number and the "*n*" denotes the subband-state number in the QW number. For example, "Γ21" and "Γ22" denote the ground ($n = 1$) and the first excited Γ subband ($n = 2$) states in the second well (Q2: $m = 2$), respectively. The *X* subband states in the wide barrier (B1) are denoted similarly with indices *X*11, *X*12, etc. The barrier height, the band-gap alignment, etc. (Fig. 2), are properly adjusted to clearly show the potential profile within the limited space of the figures. Below we use similar scaling for the figures regarding potential and wave function.

Our sample was fabricated into *p*-*i*-*n* diode mesas of 400-μm squares with alloyed Au electrodes as contacts.

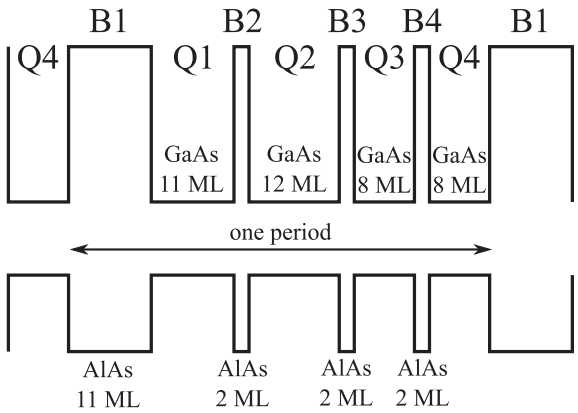

FIG. 1. Schematic illustration of potential profile of AQQW SL. Left and right sides correspond to p-cap side and n-substrate sides.

We confirmed the Ohmic contact by current-voltage characteristic measurements (Fig. 3). The built-in voltage corresponding to the flat-band condition was about 1.0 V of the forward-bias voltage when the sample was cooled to about 20 K. Hereafter, the forward bias is denoted by a "–" sign, and the reverse bias is denoted by a "+" sign. Accordingly, -1.0 V denotes the flat-band condition. The sample was irradiated by a solid-state cw laser (532 nm) from the p^+-cap layer through a 10× objective lens to excite the carriers in the intrinsic region. PL signals were detected using a cooled charge-coupled device (CCD). All PL measurements were performed at 20 K.

For the calculation of the wave-function profiles and their energy by the transfer-matrix method, we used conventional standard values of constants [8,9] and precisely calculated the energy levels and the related wave functions (the energy resolution was less than 0.01 meV). We used a built-in voltage of 1.0 V and a total intrinsic region width of 475 nm composed of a 325-nm SL area and 100 + 50-nm cladding layer width. The 50-nm addition was assumed from an expansion of the depletion layer under high applied electric fields to this sample.

III. PHOTOLUMINESCENCE PROPERTIES AND CARRIER TRANSPORT IN AQQW SL

In this section, we describe the origin of the PL branches by analyzing the carrier transport by considering the interferences and the resonances of the subbands and discuss the PL properties that were separately divided into longer- and shorter-wavelength regions. The observed PL spectra agree well with the calculated transition energies. Note that the calculation contains a nonparabolicity effect on the Γ conduction band [9].

We use the term "Stark ladder" as follows. In old SLs with uniform structure and the same QW width and barrier widths in the whole SL periods, an N Stark ladder denotes that a recombination transition occurs between the electron and the hole states separated by the N SL period. We use this N order for the Stark-ladder transition for the N-period-separated QW pair. However, unlike uniform SLs, the distance of each QW is different due to asymmetric QW systems. Similar to the conventional definition of the Stark ladder, we use a plus

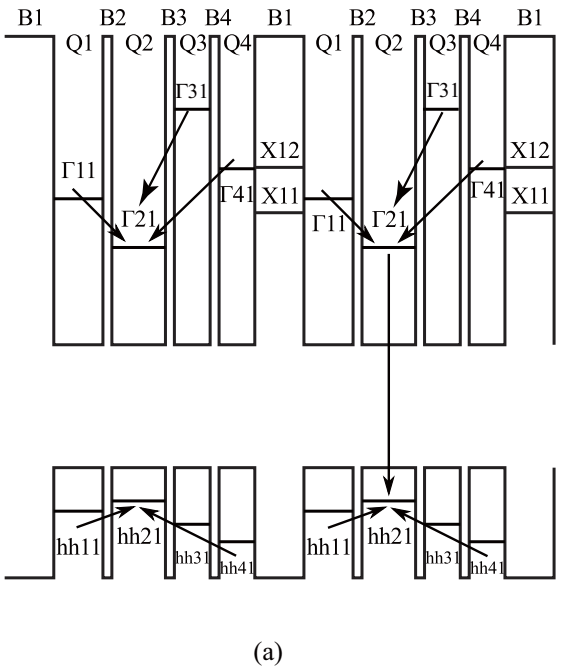

(a)

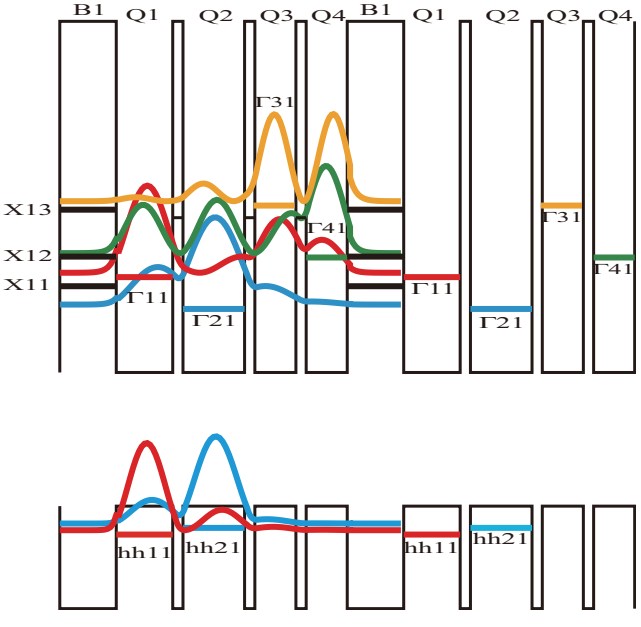

(b)

FIG. 2. (a) Schematic illustrations of hole subband energy (below) and electron energy (above). Arrows indicate relaxation of electrons to Γ21 ground state and holes to hh21 ground state, and their radiative recombination corresponds to the PL emission under the flat-band condition. (b) Calculated wave-function profile and energy level of subbands. Heavy-hole subbands of hh31and hh41 are not shown. Barrier height is reduced due to space limitations.

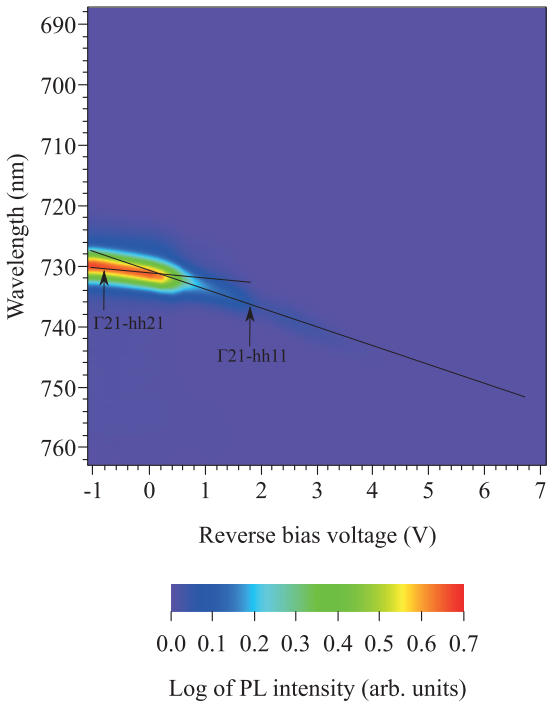

FIG. 3. Photoluminescence (PL) spectra vs reverse-bias voltage in the longer-wavelength region under 1-mW 532-nm laser excitation. Color represents logarithmic PL intensity (base = 10).

sign when the transition energy increases with increasing bias voltage. Vice versa, decreasing transition energy corresponds to a minus sign. Note that the transition between the left-side X and right-hand hole states is denoted as the $+\frac{1}{2}$ Stark ladder.

A. –1 Stark-ladder transition originating from the hole wave function in longer-wavelength region

Figure 3 shows the PL spectra as a function of the reverse-bias voltage in the longer-wavelength region. Under the flat-band condition, the photogenerated electrons in the higher-energy subbands relax to the lowest electron energy (Γ21 in Q2) [Fig. 2(a)]. On the other hand, heavy holes are concentrated in the lowest heavy-hole energy (hh21 in Q2). Therefore, we observed a Γ21-hh21 intense recombination transition at a lower bias voltage. Under a reverse-bias voltage of less than 0.2 V, the Γ21-hh21 transition is strong since most electrons and holes are concentrated in Q2. However, this PL showed a redshift from 0.2 V because the transition between hh11-hh21 dominates the -1 hole-originated Stark-ladder transition. Figure 4 shows the energy fan chart of the hh subbands. Around 0 V, large anticrossing between hh11 and hh21 was confirmed. The lowest heavy-hole energy above 0.2 V was displaced as hh11, which led to heavy-hole relaxation into Q1 through the 2-ML thin barrier (Fig. 5). As a result, a Γ21-hh11 -1 Stark-ladder PL was caused and observed from 0.2 V. This interesting hole-origin Stark ladder has rarely been observed in GaAs/AlAs systems. This model is also schematically shown in Fig. 6(a). From this evidence regarding the recombination transitions from electron states that will be described in the following sections under reverse-bias voltages exceeding 0.2 V, the recombination target is the hh11 in Q1

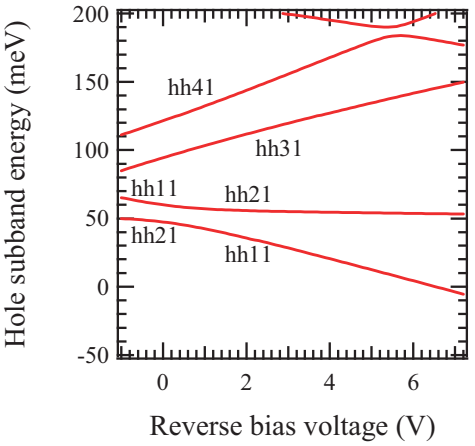

FIG. 4. Hole subband energy fan chart based on QW2. Energy fan chart is calculated based on standard QW of QW2, since hh is initially gathered in QW2 under flat-band condition. In the QW2 base case, subband state in QW2 shows little or no energy change.

(not hh21), since most of the holes have moved into the hh1. Therefore, when an electron state in the Q1 ($X11$ or Γ11) is prepared for electron occupation to recombine with the hole, and when the Γ-X mixing is accomplished for the $X11$, recombination will only occur with the hh11.

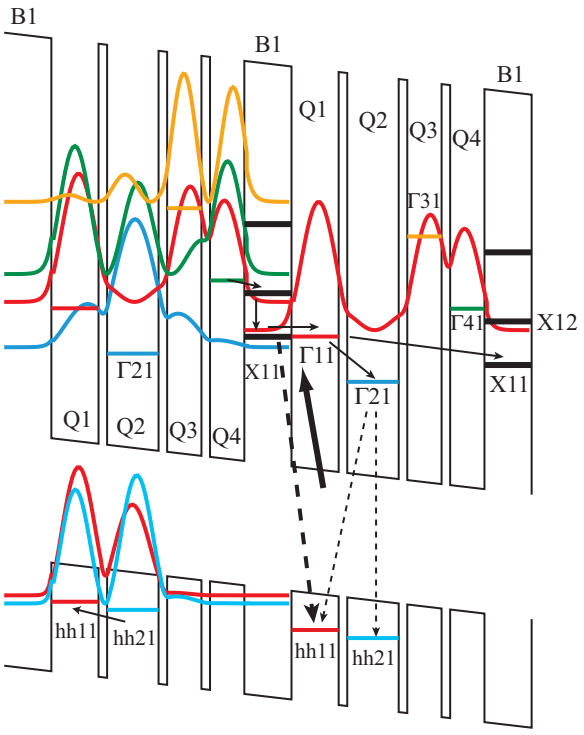

FIG. 5. Schematic illustrations of Γ11-$X11$ resonance and wave-function (probability density) profiles at 0.3 V. Arrows indicate carrier transport. Thick lines with arrow indicate Γ-X mixing point. Thick dashed arrow indicates radiative recombination from Γ11-$X11$ mixed state to hh11. Dotted lines with arrows indicate radiative recombination from Γ21 at bias voltage lower than 0.3 V.

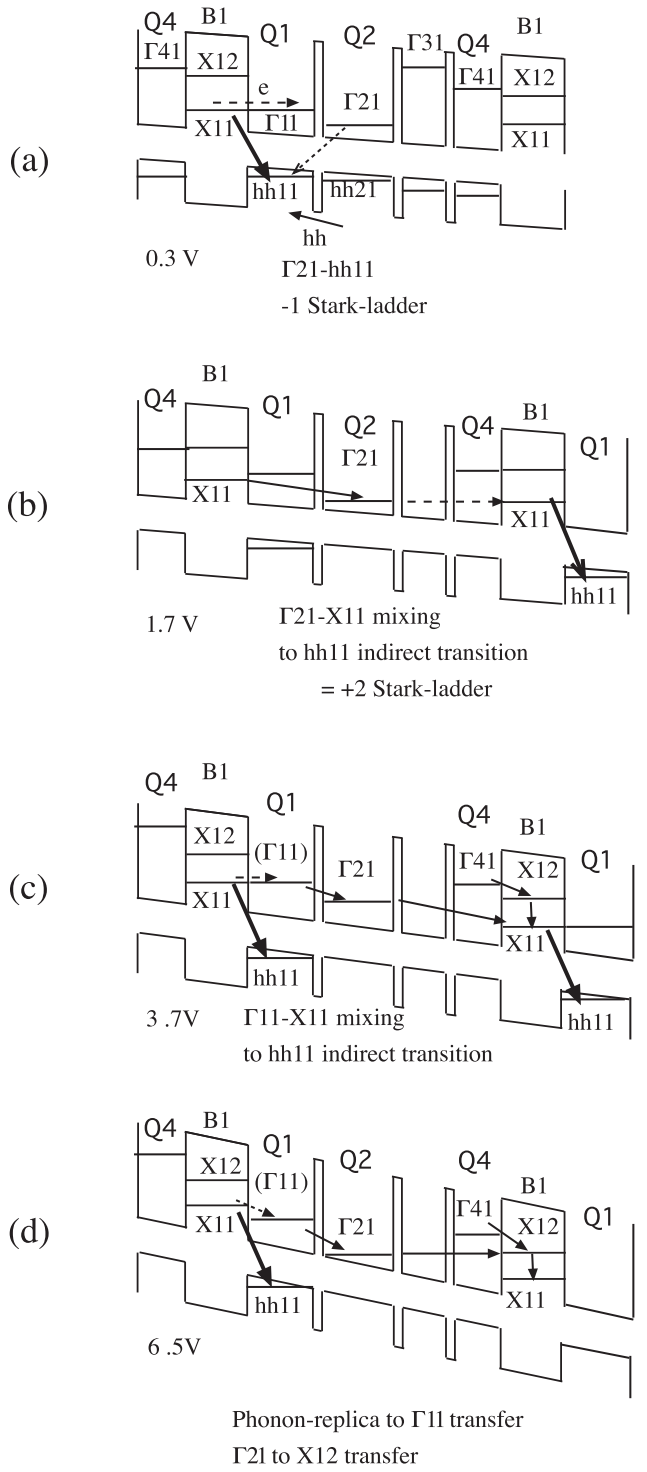

FIG. 6. Schematic illustration of electron transport and resonances at each characteristic bias voltage.

B. PL in shorter-wavelength region and feature of the AQQW SL system

Figure 7 shows the PL spectra as a function of the reverse-bias voltage in the shorter-wavelength region. Since we found a shift of the PL profile as well as the *I-V* curve toward higher voltage under larger laser excitation power than 1 mW, we used 1-mW power in order to not deform their

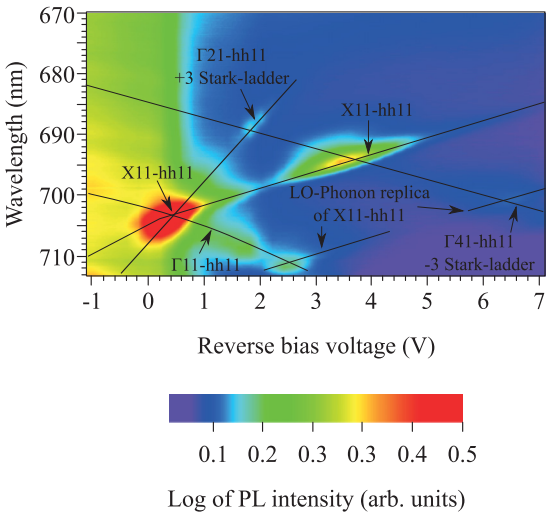

FIG. 7. Photoluminescence (PL) spectra vs reverse-bias voltage in shorter-wavelength region under 1-mW 532-nm laser excitation. Color represents logarithmic PL intensity (base = 10). The integration time of the cooled-CCD detector is ∼100 times longer than that for Fig. 3 to detect weak PL.

voltage dependence heavily. This shift in externally applied bias voltage comes from space-charge screening of the electric field in SL generated by the number of electrons trapped in the *X*11 state.

To resolve such strange PL spectra in Fig. 7, we calculated and analyzed the interferences among electron subbands, the electron transfer schema, and the resonances of the electron subband energies in the fan chart in Figs. 6 and 8. In Fig. 8, three resonance points, which are marked by solid circles, are the Γ-*X* crossing points of the higher Γ electron states, where anomalous PL emissions are observed in Fig. 7. In Fig. 8,

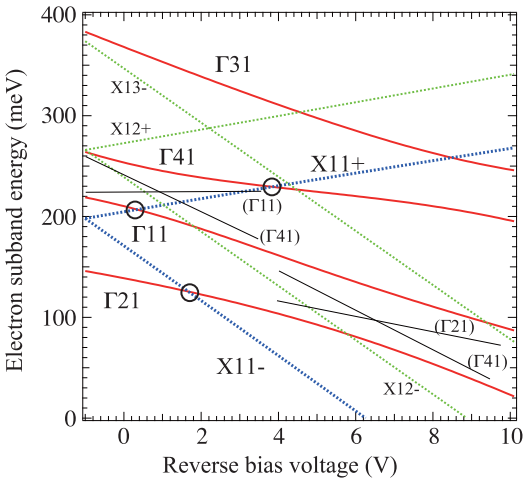

FIG. 8. Electron subband energy fan chart based on QW1, since radiative recombination shown in Fig. 7 occurred with hh11 in QW1. Thick solid curves are Γ ground states in four QWs. Dotted lines are *X* subbands in the 11-ML barrier B1. Crossed thin lines indicate anticrossings. Higher-electron-energy states are not shown, since little or no electron occupation is expected due to relaxation to lower-energy states.

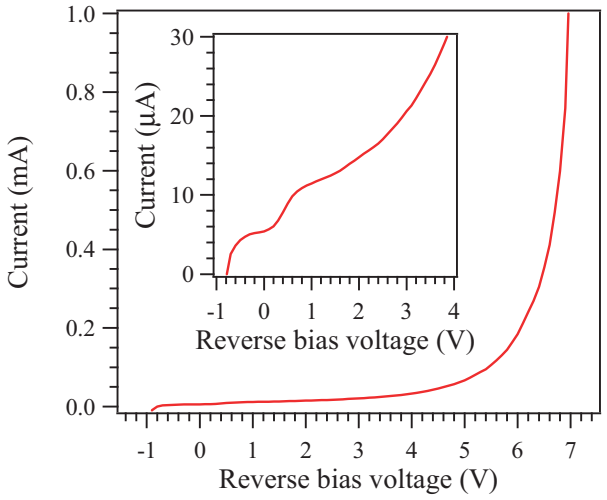

FIG. 9. Current vs reverse-bias voltage characteristics (*I-V* curve) of sample under 1-mW laser excitation intensity. Inset shows detailed *I-V* curve below 4 V.

the red solid lines are the Γ states in QW, the blue dotted lines are the *X*11 state in the barrier B1, and the green dotted lines indicate the *X*12 and *X*13 subbands in the B1 barrier. Since other subband energies exceed the top energy of this figure and no electron occupation seems to exist, we omit those energy fan charts. The thin solid black lines indicate the anticrossings between the Γ states. Since the barrier width separating each QW is very thin (2 ML), we observed large anticrossings (large energy splittings), which is a feature of this AQQW SL system. Especially for Γ41 and Γ31, since both the QW widths of Q3 and Q4 are equal, the strong interference of the wave functions greatly splits their energies under the flat-band condition, as shown in Figs. 2(b) and 8. Without any interference, both energy levels would be equal.

The anticrossing between Γ11 and Γ41 occurs at ∼1 V, confirmed by the change of the wave-function profiles of the states. Next the anticrossing change of the subband state occurs. Γ41 is replaced by Γ11, and vice versa, as indicated by the subband names in parentheses in Fig. 8. Since Γ11 was replaced by Γ41, the replacement after anticrossing at 6.4 V generates (Γ21) and (Γ41). However, the subband states that were interfered with at the anticrossing points are heavily mixed as indicated by the large energy splittings. These things are explained in the following discussions by the wave-function profiles, which show widespread distribution through multiple QWs. Therefore, the (Γ11) and (Γ41) states resemble a mixed state of Γ41 and Γ11. The (Γ21) and (Γ41) case is similar. The anticrossing point between (Γ11) and Γ31 is ∼10 V (not shown in Fig. 8), since the phenomenon occurs at a very high voltage and does not affect our discussion.

Figure 9 shows the current-voltage characteristics (*I-V* curve) of the sample, which shows the steep increase of the output current after ∼6 V, causing a breakdown of the device. This is why the PL and *I-V* curve measurements stopped at 7 V. The origin of the current increases in the *I-V* curve will be clarified later. Figure 6 schematically shows the carrier transports and the resonances at these characteristic voltages.

C. PL branches originating from subband resonances among higher-energy subbands

Next, we analyze the PL spectra in Fig. 7. The PL peak around 0.4 V and 705 nm comes from the *X*11(+1/2)-hh11 Stark-ladder transition. Heavy holes have already been transferred into hh11 in Q1 from 0.2 V. On the other hand, in Fig. 5, electrons have been trapped into the *X* state in the B1 barrier through relaxations from the Γ subbands, except for the Γ21 having lower energy than the *X*11. From Fig. 8, the Γ11 and *X*11 energies are matched at 0.3 V, which causes Γ-*X* mixing and enables PL emission from the *X*11 state. Since a recombination transition occurs between the left-side *X*11 and the right-side hh11, the transition energy is increased with increasing bias voltage [Fig. 6(a)], and thus a PL branch along the *X*11+ line in Figs. 7 and 8 is observed. In Fig. 7, the PL is emitted around the crossing point between the Γ11 and *X*11+ calculated lines (both hh bases have the same hh11, since the electrons recombine with hh11). Therefore, our calculated results in Figs. 5, 7, and 8 agree well with the experimental result, and can resolve the origin of this PL peak.

Below the 0.3-V bias, since the lowest-energy Γ state is Γ21, most of the electrons relax down in the Γ21 and emit PL by the Γ21-hh21 transition. From 0.2 V, the hh moves to hh11 and the Γ21-hh11 -1 Stark-ladder PL starts to be observed. However, the PL intensity is weak although the overlap integral is sufficiently large, as shown by the blue wave-function profiles of the Γ21 and hh11 in Fig. 5. This is because the hh occupation in hh1 is consumed by the *X*11(+1/2)-hh11 recombination after 0.3 V (Fig. 5). The electron occupation in the *X*11 state seems very large since the density of state is much larger than that of the Γ states [9]. Therefore sufficient electrons, relaxed from the higher-energy Γ states, might be trapped in the *X*11 state. In addition, as shown in Fig. 5 by the long horizontal solid line with the arrows pointing to the right, the transferred electrons from *X*11 into Γ11 (figure's center) can effectively move into the *X*11 state in the next B1 barrier since a high peak of the probability density of the Γ11 wave function (red curves) only exists in the left adjacent position, which suggests that the electron in the Γ11 state also simultaneously exists in the Q4 (the rightmost QW in the figure) from the quantum mechanics theory. Therefore, this long-range *X*-Γ-*X* transfer increases the efficiency of the electron transport. The *I-V* curve (Fig. 3, inset) shows a sharp increase of the output current after 0.4 V because the Γ11 wave function is spreading widely in the one SL period that comes from mixing of the Γ11 state with Γ41, described in Sec. III B. The long-range transfer is from the Γ11 state in Q1 to the *X*11 state in the B1 barrier, which is the electron transport that starts from Q1 through Q2, Q3, and Q4 to the *X*11 state: a long-distance transfer. We believe that this long-range *X*-Γ-*X* transfer is an interesting phenomenon in semiconductor physics. When using a GaAs/AlAs AMQW with very thin barriers, a long-range Γ-*X* transfer cannot be ignored. This might be a key point in the future design of quantum-cascade structures in GaAs/AlAs systems.

D. Anomalous redshift in the Γ11-hh11 transition

A downward PL, marked as Γ11-hh11 at around 1.4 V and 708 nm that appeared after the above Γ11-*X*11 resonance in

Fig. 7, is the Γ11-hh11 transition. Remarkably, the observed Γ11-hh11 PL spectra showed an anomalously large redshift that was greater than expected from the quantum confined Stark effect (QCSE) in conventional thin QW-width systems (in our case, 11-ML QW.) This anomaly can be solved as follows. Since Γ11 suffers interference from Γ41 and exhibits large anticrossing, the energy shows a large decrease (Fig. 8). Electrons are supplied from *X*11 by a relaxation process. Since the electrons in the Γ11 state (even after the long-range *X*-Γ-*X* transfer) are consumed by this PL as well as the relaxation into the Γ21, the increase of the output current is not so large (Fig. 3).

At about 2.1 V, the PL intensity drops by electron trapping into the *X*12 by Γ11-*X*12 resonance and transfer (Fig. 8). After 2.1 V, most of the electrons in the higher-subband states are transferred to the *X* states. However, the PL reappears at about 2.3 V, since the *X*-Γ transfer was promoted by the LO-phonon emission, which is described later in Sec. III G.

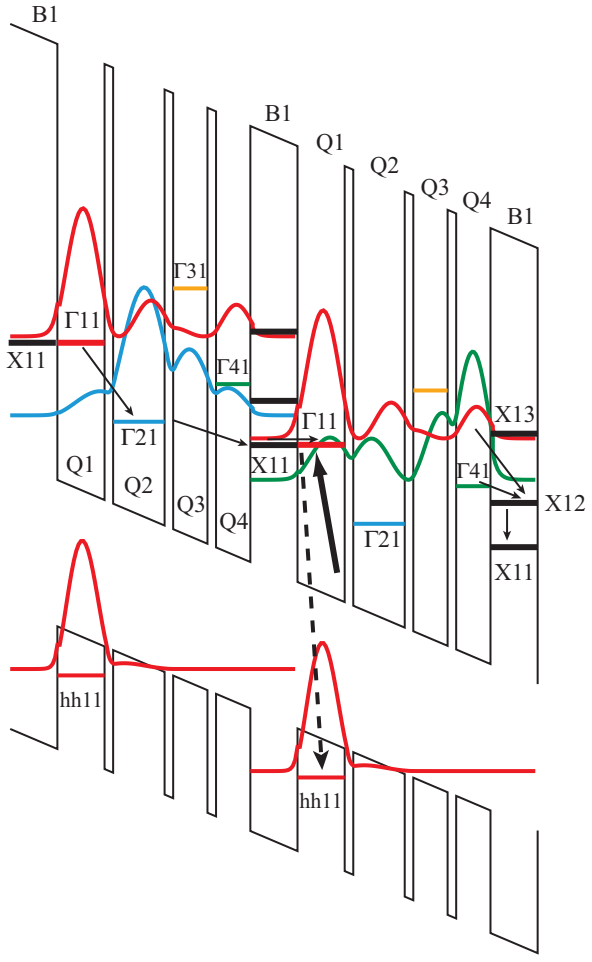

FIG. 10. Schematic illustrations of Γ11-*X*11 resonance and wave-function profiles at 3.7 V. Large wave-function overlapping between Γ11 and *X*11 generates reappearance of *X*11-hh11 transition corresponding to PL emission at around 690 nm for a bias voltage at around 3.7 V. Thick black line with arrow indicates Γ-*X* mixing. Dashed arrow indicates space indirect transition from Γ11-*X*11 mixed state to hh1.

E. PL branches originating from Γ41 -3 Stark ladder

A PL, which is derived from an *X*11(+1/2)-hh11 Stark-ladder transition reappears from 3 to 4 V, as shown in Fig. 7. Figure 10 indicates the wave-function and the energy-level profiles at the Γ11-*X*11 resonance at 3.7 V and a large wave-function peak of Γ11 at the right side QW of *X*11. Since the Γ41 and Γ11 wave functions are heavily mixed to construct a mixed state, this Γ-*X* resonance (mixing) may be interpreted as the *X*11-Γ41 resonance shown by the circle on the Γ41 curve in Fig. 8. However, the Γ41 curve is altered by (Γ11) after the anticrossing, as described in Sec. III B. Therefore, this resonance is accurately interpreted as Γ11-*X*11 resonance. In fact, the peak of the Γ wave function is located in Q1. From Fig. 8, the (Γ11)-*X*11 resonance voltage agrees well with the experimental voltage in Fig. 7. Therefore, PL reemission was observed. This scheme is also shown in Fig. 6(c), where Γ11 is represented as Γ41. In Fig. 7, the Γ41 line in Fig. 8 is denoted as a Γ41-hh11 -3 Stark-ladder line to clearly highlight the subband energy line. Here the large anticrossing with the Γ11 line is obvious and resembles that in Fig. 8. However, it becomes a (Γ11) line after the anticrossing, as noted above.

Γ-*X* mixing generates *X*11(+1/2)-hh11 Stark-ladder PL emission by a similar manner, as cited in Sec. III C. In the 3- to 4-V case, the electrons are sufficiently supplied from the higher-subband states to the *X* state in the B1 barrier after Γ21-*X*11 resonant voltage at 1.8 V as will be described

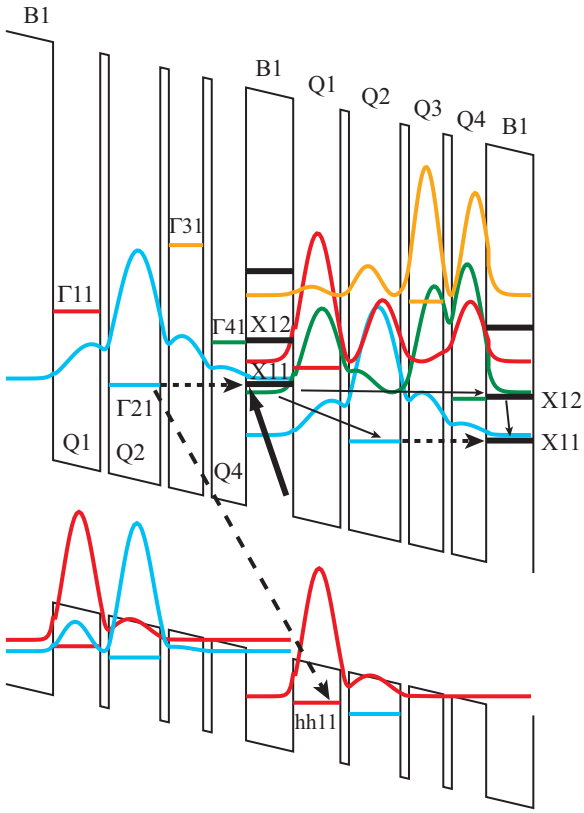

FIG. 11. Electron subband energy fan chart at 1.7 V. Dotted lines with arrow indicate Γ21-*X*11 resonance. Thick black line with arrow indicates Γ-*X* mixing. Dashed arrow indicates space indirect transition from Γ21-*X*11 mixed state to hh1.

in Sec. III F, following. Since Γ21 is the lowest Γ subband, the relaxed electrons from the higher Γ subbands are stored in the Γ21. When Γ21-*X*11 resonance occurred, the stored electrons in Γ21 can be transferred to *X*11, which promotes large electron occupation in the *X*1. In addition, the Γ11-*X*12 resonance after 2.1 V may promote carrier occupation in *X*11, since *X*12 to *X*11 is rapid due to the same *k*-vectors of the *X* states.

By this Γ-*X* mixing and transfer, the current output is further increased, as shown in the *I*-*V* curve in the inset of Fig. 9, due to the opening of several electron transfer paths as well as the (Γ11)-*X*13 path at about 4.5 V [Figs. 6(c), 8, and 10]. The (Γ11)-*X*13 path might be one cause of the decrease of the $X11(+\frac{1}{2})$-hh11 Stark-ladder PL after 4 V.

F. PL branches originating from Γ-*X* mixing with remote Γ state

In the above sections, the Γ-*X* mixing is caused by subband mixing between just the right-side adjacent Γ state and the left-side *X*11 state. In this section, we show another type of Γ-*X* mixing.

Around 1.8 V and 690 nm, we observed an odd PL with a large blue shift labeled "Γ21-hh11 +3 Stark ladder" (Fig. 7). The origin of this transition is shown in Fig. 6(b), and the wave function and energy are shown in Fig. 11. The electrons in the Γ21 state can escape into *X*11 due to the Γ21-*X*11 resonance in this voltage range. The large blueshifted PL (i.e., with a high plus Stark-ladder index) suggests a transition between the large spatially separated subband states and the electron state and the left and right sides of the hh state position, respectively. Since Γ21 is the lowest Γ subband in this voltage, we expect that many electrons will be relaxed down from the higher-energy states and stored into this state and seek an escape path. If an escape path is established, many electrons will rush the path even though the probability is relatively small. This is the Γ21-*X*11 path indicated by the horizontal dashed arrows in Fig. 11. Since relatively many electrons contribute to this process, a weak but observable PL can be detected, as Fig. 7 suggests. Since the calculated energy and voltage in Figs. 7, 8, and 11 agree well with the experimental data in Fig. 7, these experimental PL data strongly support the evidence of the Γ21-*X*11 mixing and transfer. Much electron occupation in the *X*11 has already been guaranteed by the *X*11-Γ41-*X*12-*X*11 transfer at this voltage (Fig. 11).

An interesting point is that a remote subband state far from the *X* state can generate Γ-*X* mixing when the separating barriers are very thin. The mixing Γ state is positioned on the left side corresponding to the *X* state, which generates a plus Stark-ladder PL with an index greater than 1. On the contrary, the recombined hh state by the Γ-*X* mixing state only exists in the adjacent right-hand side from the *X* state. This is very problematic, since Γ-*X* mixing at the left-hand side can recombine with the right-hand hh, and the PL data show evidence of this. In this circumstance, although the Γ-*X* scattering occurs locally in the vicinity of the GaAs-AlAs interfaces belonging to the B1 thick barrier, the probability density peak of the Γ wave function exists in a remote QW far from the B1 barrier. Since the wave function spreads widely through the AQQW, the Γ electron can reach the barrier interface at long-range distances, and can cause the Γ-*X* mixing or scattering. Therefore, we call it "remote Γ-*X*

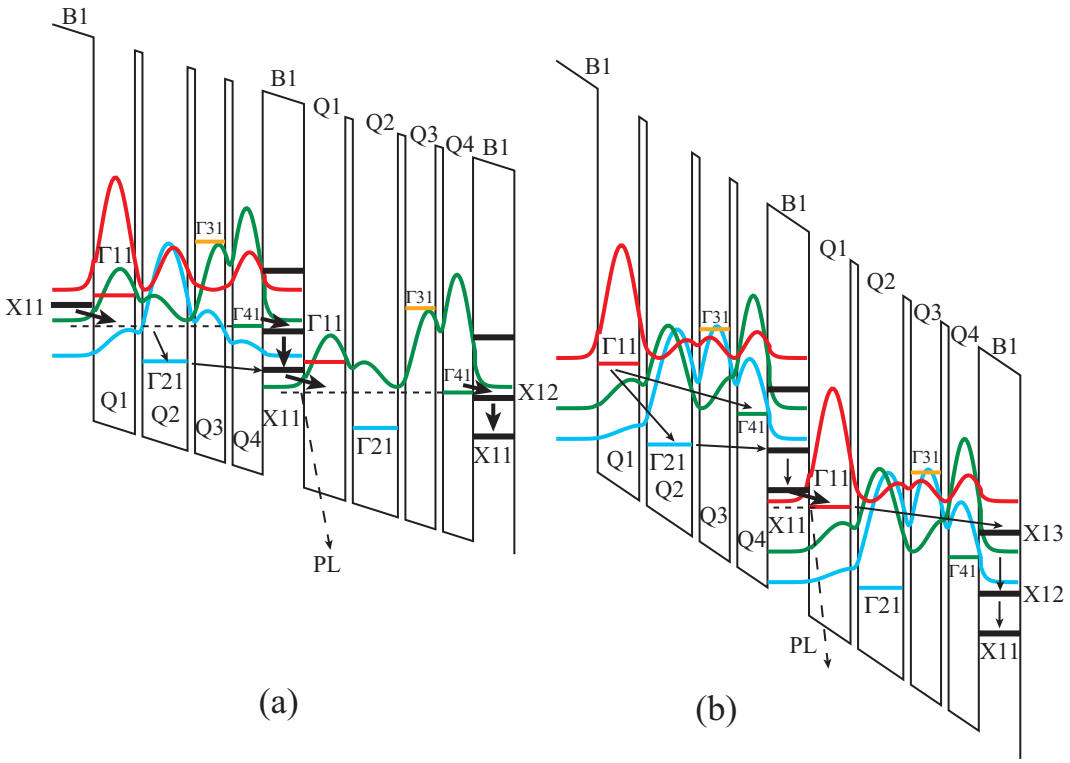

FIG. 12. Schematic illustrations of carrier transfer and wave-function profiles at (a) 2.5 V, (b) 6.5 V. Dashed lines are LO-phonon replica energy.

mixing or scattering" in this paper, since these phenomena occur between the Γ states far from the *X* state.

Such a phenomenon (remote Γ-*X* mixing) is very anomalous but interesting in semiconductor physics and may contribute to future experimental studies and theoretical developments.

G. PL from phonon replica

The last theme to be investigated is the PL branches marked as "phonon replica" [10–12] in Fig. 7. The PLs are found along the same shift gradient of the *X*11+ line and suggest that the PL emissions are related to the *X*11-hh11 PL emissions. In fact, the energy separation between the *X*11+ and the indicated phonon-replica lines at the same voltage agrees well with the LO-phonon energy in GaAs (36 meV).

The blueshifted PL line in Fig. 7 at about 2.5 V indicates *X*11-hh11 phonon replica. The *X*11 carrier occupation was caused by the *X*11-Γ11 resonance around 0.3 V in Fig. 7. The band alignment and the wave-function profile at 2.5 V are shown in Fig. 12(a). Under this circumstance, the mixing state of Γ11 and Γ41 has a wave-function peak at Q1, and then the LO-phonon-separated energy state obtains electrons from the *X*11 state and transfers them to the next *X*12 state in the next right B1 barrier. This effective transfer path might collect the electrons in the *X*11 state, which causes relatively strong PL emission between the phonon replica and the hh11 in the Q1. This indirect recombination belongs to the *X*11 + PL gradient.

Figure 12(b) shows the band alignment and the wave-function profiles at 6.5 V. Around 6.5 V, the PL from the phonon replica is also observed (Fig. 7). The Γ state is (Γ11) state altered (exchanged) after anticrossing with Γ41 state (Fig. 8). Around 2.5 and 6.5 V, the PL intensity was enhanced due to the LO-phonon-assisted relaxation from *X*11 to Γ11.

Here, note that to observe the LO-phonon-replica PL with sufficient PL intensity, the following conditions must be satisfied. As shown in Fig. 7, even though the PL from *X*11-hh1 is intense around 0.4 V and 3.5 V, no phonon-replica PLs were observed at these voltages. Although many electrons are trapped in the *X*1 state and the relaxation by LO-phonon emission to the phonon-replica state could be any amount, no PL from the replica was observed. This comes from the following physics. In simple-structured SLs, for example, and in type-II SLs under an electric field, PL intensity of the zero-phonon line is observed after Γ-*X* mixing since the phonon replica can stay in the Γ state in the adjacent QW [13]. The electrons injected into the *X* state steeply relax into the Γ state with LO-phonon emission, and emit PL with the hh in the QW. As exemplified in the PL emission process in the type-II SLs, the phonon replica does not show a PL before meeting the Γ state because the *X* electron gains a Γ component by the mixing. The above results imply the importance of the final state that must be relaxed. When the last state was just the Γ state and the wave function largely overlapped the hh state in the same QW, a relatively strong PL by phonon replica can be observed. In contrast, if the final state was an intermediate state above the Γ state, the electrons continue the relaxation by emitting acoustic phonons. Since relaxation by the acoustic phonons costs a few picoseconds, the PL cannot be observed from the zero-phonon line due to a relatively short lifetime (ps) at the state. If the electrons that relaxed into the last Γ state are not quickly swept out, the PL can be observed from this Γ state. Only when the energy of the zero-phonon line (phonon replica) was matched to the Γ state energy, was the overlap integral between the Γ and hh states large enough, and the swept-out speed was relatively small, denoting a relatively long stay in the Γ state, and a PL from the Γ state (that also corresponds to the phonon-replica line) can be observed. We also observed a similar PL from the LO-phonon replica [4].

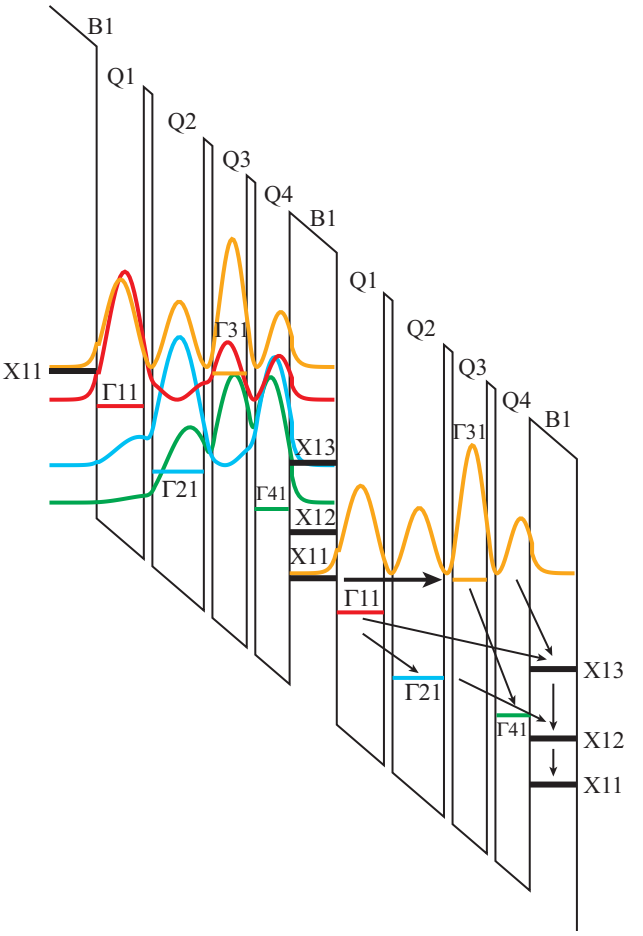

FIG. 13. Schematic illustrations of carrier transfer and wave-function profiles at 8.5 V. All ground Γ subband states contribute to electron escape to next AQQW period through *X* states in B1 barrier.

In our case, the LO-phonon replica of the *X*11 state just matches the lowest Γ state, and the electrons stay here a long enough time to allow PL emission. This case is described in this section. The phonon-replica line crosses the minus Stark-ladder line of the Γ11 state around 2.5 V, which indicates that the final state matches the Γ11 [Fig. 12(a)]. Therefore, there is no further relaxation except for the carrier transport, and thus the PL is observed as shown in Fig. 7. Around 6.5 V, the phonon replica crosses the Γ41 minus-third Stark-ladder line. In this case, since the probability density peak of the Γ41 in Q1, [i.e., (Γ11)] is very large [Fig. 12(b)], the overlap integral between the (Γ11) and the hh11 is also large. Thus, the PL along the phonon-replica line can be observed weakly, since

there are multiple fast sweep-out paths: (Γ11) to the *X*13 route and (Γ11) to Γ21 and to the *X*12 route [Fig. 12(b)].

When the probability density of the state represented by the peak of the wave-function profile was large at the right side adjacent to the B1 barrier, the relaxation from the Γ state to the *X* states in the B1 barrier is expected to be very fast, e.g., a few hundreds of femtoseconds [14]. Therefore, the sweep-out to the Γ state is fast, and the total electron transport in the AQQW period becomes very rapid [Fig. 12(b)]. This is supported by the drastic current increase from about 6 V of the experimental *I*-*V* curve in Fig. 9. Therefore, as observed in Fig. 7, a slow escape at 2.5 V shows a stronger PL than that at 6.5 V, as emerged from the estimated transport paths, by calculating the complex wave-function profiles in the AQQW with the thin barriers and the experimental current output in Fig. 9. The *I*-*V* curve in the inset of Fig. 9 also shows a sharp increase of output current due to an electron transport path in Fig. 12(a).

In our calculation, the reverse-bias voltage, which corresponds to voltage establishing the LO-phonon energy separation between (Γ11) and *X*11, was slightly higher than that of the measurement. The difference between the experiment and the calculation might reflect the influence of the number of space charges (i.e., electrons) trapped in the *X* states in the B1 barrier. These space charges may elevate the electric potential at the B1 barrier, and thus the phenomenon may occur at a slightly lower voltage than that expected from the calculation.

H. Current increase to sample breakdown

As described in the above section, the output current in the *I*-*V* curve steeply increases after 6.5 V. In this condition, three Γ states contribute to the carrier escape from the *X*11 state. This may cause the breakdown. However, the Γ31 state has not yet contributed to the escape path. If the last Γ state (i.e., Γ31) is associated with the escape path, the breakdown will have completely occurred. Figure 13 shows this scheme. At 8.5 V, the Γ31 state can resonate with *X*11, which will greatly promote electron transport. The electrons stored in *X*11 can be rapidly swept out through any transport paths as well as by Γ31. After all of the paths have been opened, electrons may quickly flow in the SL periods, which may cause a breakdown. Since hot carriers with excess high energy might be generated under a high bias voltage, the above condition could be accomplished before 8.5 V, which might be applied to start the breakdown at 7 V. We did not measure any experimental data greater than 7 V owing to the sample's breakdown. If we could measure at a bias of 8.5 V, we might be able to detect the Γ31-*XX*1+ resonance in Fig. 8.

IV. CONCLUSIONS

In this paper, we investigated the bias dependence of the PL spectra from an asymmetric quadruple QW superlattice (AQQW SL) with very thin barriers and observed interesting PL branches caused by interferences among higher-energy subbands, long-range Γ-*X* transfers, and various types of Γ-*X* mixings. We solved these by deriving them from widely spread and strongly coupled wave functions within the AQQW with a thicker barrier that separates the SL periods. In addition, we found that LO-phonon scattering, i.e., phonon replica, plays an important role in the PL emission and carrier transport properties in this structure. The most remarkable PL around 1.8 V was generated by a long-range Γ-*X*-Γ transfer and remote Γ-*X* mixing.

[1] M. H. Meynadier, R. E. Nahory, J. M. Worlock, M. C. Tamargo, J. L. de Miguel, and M. D. Sturge, Phys. Rev. Lett. **60**, 1338 (1988).

[2] M. Nakayama, K. Imazawa, K. Suyama, I. Tanaka, and H. Nishimura, Phys. Rev. B **49**, 13564 (1994).

[3] H. Kalt, *Optical Properties of II-V Semiconductors: The Influence of Multi-Valley Band Structures* (Springer-Verlag, Berlin, 1996), Chap. 4, and references therein.

[4] M. Hosoda, M. Sato, Y. Hirose, T. Shioji, J. Nohgi, C. Domoto, and N. Ohtani, Phys. Rev. B **73**, 165329 (2006).

[5] M. Hosoda, N. Ohtani, H. Mimura, K. Tominaga, P. Davis, T. Watanabe, G. Tanaka, and K. Fujiwara, Phys. Rev. Lett. **75**, 4500 (1995).

[6] N. Ohtani and M. Hosoda, Phys. Status Solidi C **4**, 353 (2007).

[7] M. Hosoda, N. Ohtani, H. Mimura, K. Tominaga, T. Watanabe, H. Inomata, and K. Fujiwara, Phys. Rev. B **58**, 7166 (1998).

[8] S. Adachi, J. Appl. Phys. **58**, R1 (1985).

[9] D. F. Nelson, R. C. Miller, and D. A. Kleinman, Phys. Rev. B **35**, 7770 (1987).

[10] M. S. Skolnick, G. W. Smith, I. L. Spain, C. R. Whitehouse, D. C. Herbert, D. M. Whittaker, and L. J. Reed, Phys. Rev. B **39**, 11191 (1989).

[11] B. A. Wilson, Carl E. Bonner, R. C. Spitzer, R. Fischer, P. Dawson, K. J. Moore, C. T. Foxon, and G. W. 't Hooft, Phys. Rev. B **40**, 1825 (1989).

[12] H. Kalt, W. W. Ruhle, K. Reimann, M. Rinker, and E. Bauser, Phys. Rev. B **43**, 12364 (1991).

[13] J. Feldmann, M. Preis, E. O. Göbel, P. Dawson, C. T. Foxon, and I. Galbraith, Solid State Commun. **83**, 245 (1992).

[14] *Optics of Semiconductor Nanostructures,* edited by F. Henneberger, S. Schmitt-Rink, and E. O. Göbel (Akademie Verlag, Berlin, 1993), Chap. I-7, and references therein.